Pressure-induced surface superconductivity in the noncentrosymmetric superconductor $PbTaSe_2$: Pressure-dependent point-contact Andreev spectroscopy

Hai Zi,[1,2] Yu-qing Zhao,[1] Ming-chong He,[1] Yu-jia Long,[2] Lin-xiao Zhao,[2] Xing-yuan Hou,[2] Huan-xing Yang,[2] Yi-feng Yang,[2,3] Lei Shan,[2,3] Zhi-an Ren,[2,3] Jian-qi Li,[2,3] Jiang-ping Hu,[2,3] Geng-fu Chen,[2,3,*] Peng Xiong,[4] and Cong Ren[1,†]

[1]*School of Physics and Astronomy, Yunnan University, Kunming 650500, China*

[2]*Beijing National Laboratory for Condensed Matter Physics, Institute of Physics, Chinese Academy of Science, Beijing 100190, China*

[3]*School of Physical Sciences, University of Chinese Academy of Sciences, Beijing 100190, China*

[4]*Physics Department, Florida State University, Tallahassee, Florida 32306, USA*

(Received 10 June 2023; revised 11 December 2023; accepted 19 December 2023; published 20 February 2024)

A notable characteristic of $PbTaSe_2$, a prototypical noncentrosymmetric superconductor (NCS), is that its superconductivity can be modulated through a structural transition under hydrostatic pressure [Kaluarachchi *et al.* Phys. Rev. B **95**, 224508 (2017)]. Here we report on a combined pressure-sensitive point-contact Andreev reflection (PCAR) spectroscopy with bulk resistance measurements on $PbTaSe_2$, to elucidate the nature of the surface and bulk superconductivity and their evolution with hydrostatic pressure. It is found that in a high-pressure region the superconducting gap opening temperature T_c^A is significantly lower than the bulk resistive transition temperature T_c^R, revealing a clear experimental signature of surface-bulk separation associated with enhanced antisymmetric spin-orbit coupling (ASOC). The PCAR spectra, reflecting the superconducting surface state, are analyzed with two-dimensional Blonder-Tinkham-Klapwijk theory, yielding an isotropic *s*-wave full BCS gap in the strong-coupling regime. These results suggest the coexistence of full gap *s*-wave superconductivity and topological surface states in $PbTaSe_2$, indicating that this NSC superconductor with significantly enhanced ASOC may offer a solid platform to investigate the topological aspect in the superconducting condensate.

DOI: 10.1103/PhysRevB.109.064510

I. INTRODUCTION

The discovery of superconductivity in topological matters has stimulated intense interest in topological superconductors (TSCs) that may harbor exotic electronic excitation, such as Majorana fermion zero modes. Analogous to topological insulators where strong spin-orbit coupling (SOC) causes bulk band inversion, creating a surface state with a Dirac band dispersion, TSCs are characterized by nontrivial symmetry-protected surface states hosting a Dirac dispersion as well as helical spin polarization [1–10]. For realization of such an intriguing superconducting topological surface state (TSS), intrinsic TSCs exhibiting chiral *p*-wave pairing are a natural choice [11–14]. However, *p*-wave superconductivity is extremely rare and fragile in real materials, and the same is expected for the chiral *p*-wave pairing-engendered surface states. Two alternate pathways to more robust superconducting TSSs have been proposed: (i) a superconducting surface state induced by proximity coupling between a strong topological insulator and an *s*-wave superconductor [2], (the $Bi_2Se_3/NbSe_2$ heterostructures are a notable example [15–17]; and (ii) intrinsic proximity-induced surface states in a superconductor hosting strong SOC. For the latter case, a noncentrosymmetric superconductor (NCS) under certain circumstances provides a promising route to the physical realization of a TSS [6,10,18]. In the NCS, the absence of a center of inversion symmetry in the crystal structures introduces an asymmetric potential gradient and, consequently, an antisymmetric spin-orbit coupling (ASOC) [19,20]. The ASOC can lift the twofold spin degeneracy of the electron band, giving rise to a TSS and allowing an admixture of spin-singlet (even parity) and spin-triplet (odd parity) pairing components, with a mixing ratio tunable via the ASOC strength. Hence, an NCS with predominant spin-triplet pairing can be a bulk TSC, whereas an NCS with spin-singlet pairing in the bulk can still lead to a TSC on the surface if fully gapped superconductivity is induced on the TSS. An NCS with a superconducting TSS is, therefore, an intriguing platform for TSCs. Partly motivated by these theoretical proposals, a number of NCSs have been synthesized recently to provide many potential platforms to investigate the ASOC-associated topological superconductivity [21–25].

Among NCSs, chemically stoichiometric $PbTaSe_2$ has emerged as a strong candidate for a TSC [25]. Surface-sensitive angle-resolved photoemission spectroscopy has revealed that $PbTaSe_2$ possesses a fully spin-polarized Dirac surface state [26], consistent with the theoretical calculations [25]. A recent scanning tunneling microscopy/spectroscopy study [27] reported two spin-polarized Dirac TSSs on the Pb-terminated surface that also could be fully gapped at low temperature together with the bulk counterpart. The surface states exhibit essentially identical superconductivity, i.e., the

*gfchen@iphy.ac.cn
†cren@ynu.edu.cn

same gap size and critical temperature T_c as those of the bulk state. This is in contrast to the theoretical expectation that the superconducting gap or/and T_c on the TSS should be different from that of the bulk [28]. In light of the absence of a distinct interface between the bulk and surface states in $PbTaSe_2$, it remains an experimental challenge to discern their contributions to superconductivity in tunneling spectroscopies. As far as the superconducting order parameter is concerned, there exists no clear experimental evidence for a superconducting surface state which is unambiguously distinct from the bulk state. One possible reason for the absence of a distinct superconducting surface state is that the extent of inversion symmetry breaking in $PbTaSe_2$ under ambient conditions may not be significant enough to induce a large SOC and a discernible surface-bulk separation. Recently, pressure-dependent electrical transport measurements in $PbTaSe_2$ revealed two distinct types of superconductivity at high hydrostatic pressures associated with a subtle structural transition [29,30]. The observations point to an intriguing opportunity for exploring ASOC-enhanced and bulk-separated surface topological superconductivity in this high-pressure phase.

In this work, we performed planar point-contact Andreev reflection (PCAR) spectroscopy combined with bulk resistance measurements on $PbTaSe_2$ single crystals under quasihydrostatic pressures. In the high-pressure phase, the PCAR spectra revealed a superconducting gap opening temperature substantially lower than the bulk resistive transition temperature. The results present compelling evidence for distinct surface-bulk separated superconducting states, which likely originated from the enhanced ASOC strength due to the pressure-modified structural transition.

II. EXPERIMENTAL DETAIL

High-quality single crystals of $PbTaSe_2$ were grown by chemical vapor transport by using iodine as a transport agent. The details of single-crystal growth and physical property characterization are reported elsewhere [29,31,32]. The crystal structure and its noncentrosymmetric nature have been examined by scanning transmission electron microscopy (STEM) along the [001] zone-axis direction with high resolution. Specimens for TEM observation were prepared by gently crushing the single crystals into fine fragments in an agate mortar, which were then supported by a copper grid coated with a thin carbon film. STEM observations were performed in the JEOL ARM200F microscope equipped with double aberration correctors and operated at 200 kV. Under this condition, the spatial resolution is about 0.08 nm. Figure 1(a) shows typical STEM images of $PbTaSe_2$ taken along the [001] zone-axis direction. The brightness for an atomic column in the STEM photograph is proportional to atomic density in the column; therefore, the relatively brighter dots in the present image correspond to the projections of the Pb/Se columns, and the small bright dots are the atomic images of the Ta columns and agree well with the structural model. The image and corresponding diffraction pattern clearly show the high quality of the as-made sample and the noncentrosymmetric structural feature.

Samples were pressurized in a piston-cylinder clamp cell made of Be-Cu alloy 25 with the inner jacket made of alloy MP35N and Daphne 7373 as the pressure transmission medium. A calibrated Cernox thermometer attached directly on the cell close to the junction was used for thermometry. For each measurement run, the pressure inside the cell was determined by monitoring the magnitude change of the critical transition temperature T_c of the lead thin wire in a four-probe measurement.

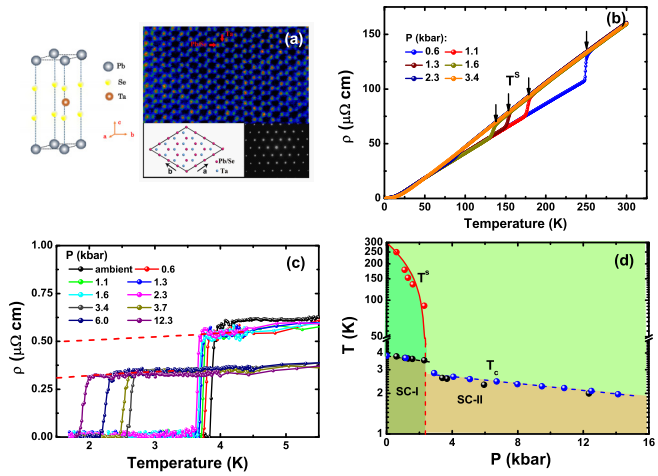

FIG. 1. (a) Characterization of the crystal structure of the $PbTaSe_2$ samples. The red arrows in the main panel point to Pb(Se) and Ta atoms' locations in the high-resolution scanning transmission electron microscopy image. The scale bar is 2 nm. The insets at the bottom are the corresponding structural model (left corner) and electron diffraction pattern (right corner), respectively. (b) In-plane ρ verse T in the full measurement temperature range under various hydrostatic pressures. (c) In-plane ρ vs T under various P values in the superconducting transition region. The red dashed lines are the extrapolation to $T = 0$. (d) The resulting $P - T$ phase diagram for $PbTaSe_2$ on a semilog scale. The dashed lines are guides to the eye.

III. RESULTS AND DISCUSSIONS

The temperature dependence of the resistivity $\rho(T)$ of the $PbTaSe_2$ single crystal under various pressures (P) is shown in Fig. 1(b). At ambient pressure, the residual resistivity ratio $RRR \equiv \rho(300K)/\rho(4K)$ is about 290, showing the high quality of our $PbTaSe_2$ samples. These P-dependent $\rho(T)$ curves are typical of those reported in the literature [29,30]: Upon the application of pressure, a steep drop of ρ occurs at temperature T^s indicated by the arrows, clearly dividing $\rho(T)$ curves into two branches of low-ρ and high-ρ states. With increasing P, T^s decreases and the ρ drop is gradually suppressed and disappears at $P > 2.3$ kbar. A detailed experiment by Kaluarachchi *et al.* reveals a thermal hysteresis between high-ρ and low-ρ phases at around T^s for $P < 2.4$ kbar, implying a subtle crystal structure modification from the high-ρ $P6m2(1e)$ phase to the low-ρ $P\bar{6}m2$ phase [29]. In comparison to the $P\bar{6}m2$ phase, the high-ρ $P6m2(1e)$ phase displays a sizable contraction in the c axis while the a axis is slightly expanded, leading to an enhanced noncentrosymmetry.

The P-induced structure transition at T^s in $PbTaSe_2$ shows a distinct correlation with its superconductivity at low

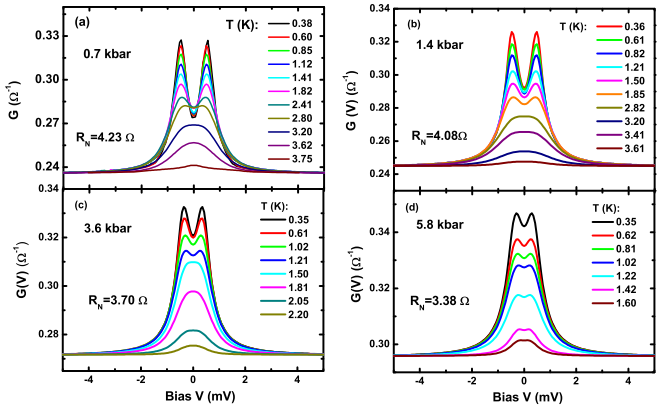

FIG. 2. Evolution of the planar point-contact Andreev conductance spectrum $G(V)$ of $PbTaSe_2/Ag$ (J1) as a function of T under various pressures. The labeled junction resistance R_N is defined based on the conductance values at high bias voltages in the normal state.

T values. As shown in Fig. 1(c), a blow-up of resistance in the superconducting transition regime clearly splits into two superconducting transition branches. In the low-P region (high-ρ branch, $P < 2.3$ kbar), the sample shows sharp superconducting transitions with T_c varying little with pressure (SC-I). In contrast, pressures above 2.9 kbar result in a substantial decrease in the residual resistance, accompanied by large suppression of T_c, suggesting a different superconducting state with an enhanced ASOC strength under high pressure (SC-II). These results of T^s and T_c are used to construct the $T-P$ phase diagram shown in Fig. 1(d), which indicates two distinct superconducting phases separated by a structural transition. First-principle calculations also point to the structural origin for this Lifshitz transition without any change of global symmetry [30]. Another piece of evidence for enhanced ASOC in SC-II comes from the observation of much lower T_c values in this high-P phase (SC-II) with otherwise similar structural parameters, suggesting that a strong ASOC is detrimental to superconductivity [33,34].

We utilized the P-dependent PCAR spectroscopy technique to explore the nature of superconductivity in $PbTaSe_2$ in the SC-II region [35–37]. The P-dependent PCAR spectra provides unique insights into the effect of the enhanced ASOC on the nature of the NCS superconductivity across the critical pressure of $P_c \simeq 2.5$ kbar. The high-pressure PCAR measurements on $PbTaSe_2$ crystals were made possible by "soft" point contacts made using a thick silver paste and bonding with Pt wires to the flat and shiny surface cleaved along the c axis of $PbTaSe_2$ crystals [38]. Details of the point-contact fabrication and the nature of these point-contact can be found in the Supplemental Material SI [39] (see also Refs. [40–43] therein). It was demonstrated that the "soft" point contact has the advantage of avoiding inhomogeneous local pressure effects induced by a metal-tip [44–46]. More importantly, there are growing pieces of evidence in experiments for detecting surface state superconductivity by the "soft" Andreev reflection spectroscopy technique due to its surface-sensitive nature [44,47,48],

Figure 2 shows the raw conductance curves, $G(V) \equiv dI(V)/dV$, of a c axis $PbTaSe_2/Ag$ point contact (J1) as a function of T under several quasihydrostatic pressures spanning P_c up to 5.8 kbar. To ensure the reliability and reproducibility of the P-dependent spectra, we measured the conductance spectra of another $PbTaSe_2/Ag$ point-contact (J2) up to 12.1 kbar (see Supplemental Material SII [39] and Ref. [37]). As displayed, several features of the conductance are worth noting. (i) The spectra show a systematic evolution with the variation of P across the P_c. The pronounced double-peak at the gap edges at low P is gradually suppressed with increasing P, implying increased junction transparency and the dominance of the AR process. (ii) The $G(V)$ curve becomes flat and featureless as T approaches T_c, and it overlaps at high bias voltage with the normal-state curves. The well-defined double peaks at the gap edges at the lowest T values is a tell-tale signature of an s-wave-like order parameter in the superconductor. At $P > P_c$, the $G(V)$ spectrum shows a zero-bias conductance dip, instead of a peak. A zero-bias conductance peak in the junction spectrum is widely regarded as a manifestation of a p-wave nodal gap in the superconducting order parameter. The persistent presence of the zero-bias conductance dip in the high-pressure region is strong evidence against the dominance of a p-wave order parameter in the SC-II regime.

The combined determination of the P-dependent point-contact conductance spectra and the bulk transport properties offers the intriguing possibility of discerning surface-bulk separation by examining the superconducting order temperatures of the surface and bulk states. In principle, the Andreev reflection is manifested as the conductance enhancement in $G(V)$, especially the zero-bias value $G(0)$, above the normal-state counterparts. A superconducting gap opening/closing temperature, T_c^A, is defined as the temperature at which the Andreev conductance features disappear and the conductance spectrum becomes indistinguishable from that of the normal state. In this criterion, T_c^A falls within the width of the superconducting fluctuation region which defines the bulk superconducting transition temperature T_c^R in the $\rho(T)$ curve for conventional superconductors. In Fig. 3, we present both the zero-bias PCAR conductance $G(0)$ and the simultaneously measured bulk resistance of the $PbTaSe_2$ crystal as functions of temperature under various P values. For all P's, $G(0)$ shows a clear transition from sharp variation with T to almost T independent, making the identification of T_c^A straightforward. As shown in Figs. 3(a) and 3(b), in the low-P regime ($P \simeq 0.6$ and 1.4 kbar), the gap opening temperature ($T_c^A \simeq 3.8$ and 3.76 K, respectively) identified from $G(0)$ exactly matches the superconducting-resistance transition temperature T_c^R, which is defined as the zero-resistance T. In contrast, above P_c in the SC-II state, as shown in Figs. 3(c) and 3(d) at $P = 3.6$ and 5.8 kbar, respectively, there exists a clear bifurcation of T_c^A from $G(0)$ and T_c^R from $R(T)$. For example, for J1 at $P = 3.6$ kbar [Fig. 3(c)], $T_c^A \simeq 2.25$ K, far below the $T_c^R = 2.80$ K of the $R(T)$ curve. The same is true for J2, at $P = 5.2$ kbar [Fig. 3(e)], $T_c^A \simeq 1.9$ K, far below the $T_c^R = 2.50$ K of the $R(T)$ curve. In Fig. 3(g), we construct a superconducting $T_c - P$ phase diagram based on the data of T_c^A and T_c^R from these measurements and those of T_c^R obtained from the $R(T)$ curves in Fig. 1(d). Here, we emphasize that the simultaneous PCAR and $R-T$ measurements in our experiment eliminated random errors in the pressure determination. It is evident that

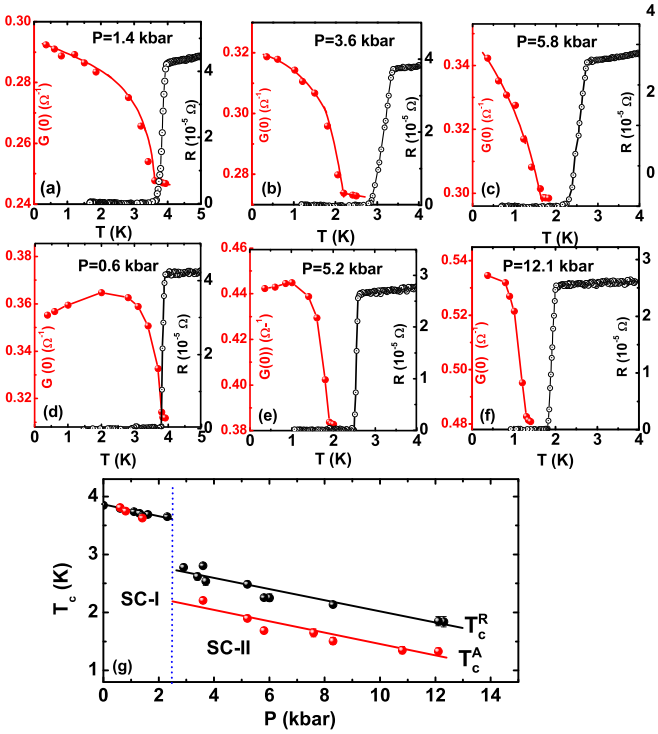

FIG. 3. Comparison of the superconducting ordering temperature T_c measured using T dependence of the zero-bias conductance, $G(0)$, of the $PbTaSe_2$/Ag planar point-contact spectra (red solid dots) and the superconducting resistive transition $R-T$ curves (black open circles) of a $PbTaSe_2$ crystal from the same patch. (a)–(c) For contact J1; (d)–(f) for contact J2. (g) The summarized superconducting ordering temperature T_c in a $T-P$ phase diagram. The red solid circles are T_c^A, and the black open circles are T_c^R. The black and red solid and dotted blue lines are guides to the eye for T_c^R and T_c^R, respectively.

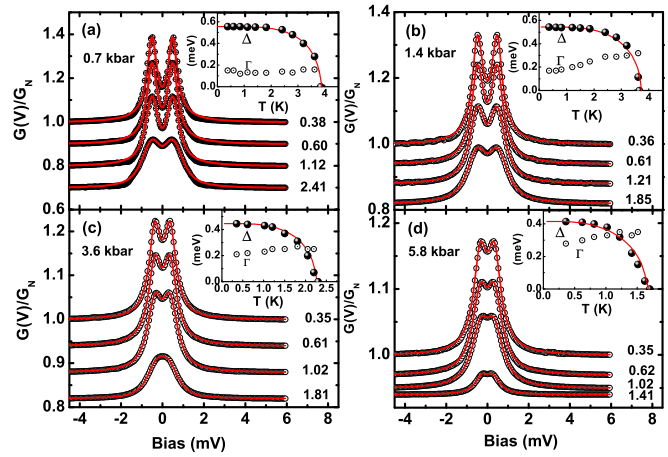

FIG. 4. Normalized $PbTaSe_2$/Ag planar point contact Andreev conductance spectra, $G(V)/G_N$, under four Ps as functions of T. The red solid lines are BTK-model fits based on a single s-wave gap. The $G(V)/G_N$ curves with their fits are shifted downwards for clarity except for the ones at the lowest Ts. Insets: The superconducting gap values Δ and the spectral broadening parameter Γ from the BTK fits as functions of T, respectively. The red solid lines are BCS fits.

in the SC-II region characterized by an enhanced ASOC, the T_c-P curve is split into two distinct branches, i.e., T_c^A-P and T_c^R-P lines, in contrast to the case in the SC-I state ($P<P_c$) with weaker ASOC strength. Notably, this bifurcational behavior of T_c in the SC-II region has also been observed by P-dependent magnetization-T measurement, where the critical temperature T_c^M was shown to be lower than the zero-resistivity T_c^R [29], by an amount of 0.5 K, compatible with those of our observations. Generally, there should be a large separation in energy between the bulk bands and the surface bands near Fermi level, just like the cases of Fe(Te,Se) and $CaKFe_4As_4$ [49,50]. Thus, this distinction of T_c's determined from bulk resistivity and PCAR spectrum measurements is a strong indicator of a superconducting surface state proximity induced by the enhanced ASOC strength. This is regarded as a key experimental signature of surface-bulk separation in momentum space, which also meets the theoretical requirement that there should be a large separation in energy between the surface and bulk bands near the Fermi level [2,51]. Remarkably, the signature of surface-bulk separation in pressured $PbTaSe_2$ is similar to the case of multilayer $Bi_2Se_3/NbSe_2$, in which a TSS has been verified by comparing the opening temperature T_c^A of the proximity-induced gap with that of the bulk $NbSe_2$ [48].

To quantitatively assess the nature of the superconductivity in the TSS of $PbTaSe_2$ in the SC-II state, we determine the gap function Δ by fitting the PCAR spectra to a generalized two-dimensional Blonder-Tinkham-Klapwijk (BTK) model [52,53]. Examples of the normalized $G(V)$ curves and their BTK fits at the selected T values are shown in the main panels of Figs. 4(a)–4(d) for $P=0.6$, 1.4, 3.6, and 5.8 kbar, respectively. The use of a single isotropic s-wave gap in the BTK model (red lines) yields best fits to the data, which capture very well all the important features of the experimental $G(V)$ curves. The analyses yield a set of T-dependent fitting parameters, especially the gap size, $\Delta(T)$, at different temperatures. The insets of Figs. 4(a)–4(d) are the extracted gap values as functions of T for the corresponding P values. The resulting $\Delta(T)$ are well described by the BCS gap function: $\Delta(T)=\Delta_0\tanh(\alpha\sqrt{T_c/T-1})$, where α is the coupling strength, shown as the red solid lines in the insets. Using this formula, we obtained the zero-T gaps $\Delta_0=0.56$, 0.55, 0.43, and 0.41 meV, and $T_c=3.8$, 3.75, 2.25, and 1.69 K, for $P=0.7$, 1.4, 3.6, and 5.8 kbar, respectively. It is worth noting that in this formula, the fitting parameter T_c is the critical temperature for gap opening and closing ($\Delta=0$). These T_c values are fully consistent with T_c^A determined from the zero-bias conductance $G(0)$.

In addition, the gap ratio $2\Delta/k_BT_c$ is the measure of coupling strength of the superconducting state. For a BCS superconductor in a weak-coupling limit, the gap ratio $2\Delta/k_BT_c$ is a universal constant 3.53, exactly the case of $PbTaSe_2$ at low $P<P_c$. However, for $PbTaSe_2$ with the enhanced ASOC in the SC-II region, the ratio increases with $P>P_c$, reaching 4.43 at 3.6 kbar and 5.62 at 5.8 kbar. This is in contrast to the case of a conventional strong-coupling superconductor, for example, in Pb $2\Delta/k_BT_c=4.66$, and the value decreases gradually with increasing P [54]. Our experimental results strongly suggest that the proximity-induced superconductivity in the TSSs of $PbTaSe_2$ is in the strong-coupling regime.

Further experiments, such as *P*-dependent Andreev reflection spectroscopy under magnetic fields, are needed to probe the so-called Majorana zero-energy mode on surfaces such as the topological superconductor $PbTaSe_2$ [55–57].

IV. CONCLUSIONS

We have performed combining point-contact Andreev reflection spectroscopy with bulk resistivity measurements under quasihydrostatic pressures to investigate the effect of ASOC on the superconductivity of $PbTaSe_2$. With increasing pressure, $PbTaSe_2$ experiences a structural Lifshitz transition with an enhanced ASOC in the high-*P* phase. In the high-*P* region, the superconducting-gap opening temperature T_c^A of the surface state is found to be consistently lower than the bulk resistive transition temperature T_c^R. The observation signals a surface-bulk separation and a proximity-induced superconducting TSS in $PbTaSe_2$. The induced superconductivity in the $PbTaSe_2$ TSSs is BCS-like in the strong-coupling limit. Further experiments, such as *P*-dependent Andreev reflection spectroscopy under magnetic fields, are needed to investigate the topological aspects of the superconducting condensate.

ACKNOWLEDGMENTS

The authors acknowledge discussions with Prof. Q.-H. Wang, H.-H. Wen, X. Lu, and Y. Chen and give special thanks to the reviewers for their insightful comments and suggestions which helped in improving the quality of the paper. This work is supported by the National Natural Science Foundation of China (Grants No. 11774303 and No. 11574373) and the Strategic Priority Research Program (B) of the Chinese Academy of Science. C.R. acknowledges financial support from the Joint Fund of Yunnan Provincial Science and Technology Department (Grant No. 2019FY003008), and P.X. acknowledges financial support from the National Natural Science Foundation under Grant No. DMR-1905843.

[1] X. L. Qi and S. C. Zhang, Topological insulators and superconductors, Rev. Mod. Phys. **83**, 1057 (2011).
[2] L. Fu and C. L. Kane, Superconducting proximity effect and Majorana fermions at the surface of a topological insulator, Phys. Rev. Lett. **100**, 096407 (2008).
[3] A. P. Schnyder, S. Ryu, A. Furusaki, and A. W. W. Ludwig, Classification of topological insulators and superconductors in three spatial dimensions, Phys. Rev. B **78**, 195125 (2008).
[4] J. Alicea, New directions in the pursuit of Majorana fermions in solid state systems, Rep. Prog. Phys. **75**, 076501 (2012).
[5] C. W. J. Beenakker, Search for Majorana fermions in superconductors, Annu. Rev. Condens. Matter Phys. **4**, 113 (2013).
[6] M. Sato and S. Fujimoto, Majorana fermions and topology in superconductors, J. Phys. Soc. Jpn. **85**, 072001 (2016).
[7] R. M. Lutchyn, J. D. Sau, and S. Das Sarma, Majorana fermions and a topological phase transition in semiconductor-superconductor heterostructures, Phys. Rev. Lett. **105**, 077001 (2010).
[8] A. B. Vorontsov, I. Vekhter, and M. Eschrig, Surface bound states and spin currents in noncentrosymmetric superconductors, Phys. Rev. Lett. **101**, 127003 (2008).
[9] J. Linder, Y. Tanaka, T. Yokoyama, A. Sudbo, and N. Nagaosa, Unconventional superconductivity on a topological insulator, Phys. Rev. Lett. **104**, 067001 (2010).
[10] S. Yip, Noncentrosymmetric superconductors, Annu. Rev. Condens. Matter Phys. **5**, 15 (2014).
[11] K. Catherine and B. John, Chiral superconductors, Rep. Prog. Phys. **79**, 054502 (2016).
[12] A. P. Mackenzie and Y. Maeno, The superconductivity of Sr_2RuO_4 and the physics of spin-triplet pairing, Rev. Mod. Phys. **75**, 657 (2003).
[13] L. A. Wray, S-Y. Xu, Y. Xia, Y. S. Hor, D. Qian, A. V. Fedorov, H. Lin, A. Bansil, R. J. Cava, and M. Z. Hasan, Observation of topological order in a superconducting doped topological insulator, Nat. Phys. **6**, 855 (2010).
[14] L. Fu, and E. Berg, Odd-parity topological superconductors: Theory and application to $Cu_xBi_2Se_3$, Phys. Rev. Lett. **105**, 097001 (2010).
[15] J.-P. Xu, M.-X. Wang, Z.-L. Liu, J.-F. Ge, X.-J. Yang, C.-H. Liu, Z.-A. Xu, D.-D. Guan, C.-L. Gao, D. Qian, Y. Liu, Q.-H. Wang, F.-C. Zhang, Q.-K. Xue, and J.-F. Jia, Experimental detection of a Majorana mode in the core of a magnetic vortex inside a topological insulator-superconductor $Bi_2Te_3/NbSe_2$ heterostructure, Phys. Rev. Lett. **114**, 017001 (2015).
[16] H.-H. Sun, K.-W. Zhang, L.-H. Hu, C. Li, G.-Y. Wang, H.-Y. Ma, Z.-A. Xu, C.-L. Gao, D.-D. Guan, Y.-Y. Li, C. Liu, D. Qian, Y. Zhou, L. Fu, S.-C. Li, F.-C. Zhang, and J.-F. Jia, Majorana zero mode detected with spin selective Andreev reflection in the vortex of a topological superconductor, Phys. Rev. Lett. **116**, 257003 (2016).
[17] W. Dai, A. Richardella, R. Du, W. Zhao, X. Liu, C. X. Liu, S.-H. Huang, R. Sankar, F. Chou, N. Samarth, and Q. Li, Proximity-effect-induced superconducting gap in topological surface states—A point contact spectroscopy study of $NbSe_2/Bi_2Se_3$ superconductor-topological insulator heterostructures, Sci. Rep. **7**, 7631 (2017).
[18] M. Sato and S. Fujimoto, Topological phases of noncentrosymmetric superconductors: Edge states, Majorana fermions, and non-Abelian statistics, Phys. Rev. B **79**, 094504 (2009); M. Sato and Y. Ando, Topological superconductors: a review, Rep. Prog. Phys. **80**, 076501 (2017).
[19] L. P. Gor'kov and E. I. Rashba, Superconducting 2D system with lifted spin degeneracy: Mixed singlet-triplet state, Phys. Rev. Lett. **87**, 037004 (2001).
[20] M. Smidman, M. B. Salamon, H. Q. Yuan, and D. F. Agterberg, Superconductivity and spin-orbit coupling in noncentrosymmetric materials: A review, Rep. Prog. Phys. **80**, 036501 (2017).
[21] K. Togano, P. Badica, Y. Nakamori, S. Orimo, H. Takrya, and K. Hirata, Superconductivity in the metal rich Li-Pd-B ternary boride, Phys. Rev. Lett. **93**, 247004 (2004).
[22] A. D. Hillier, J. Quintanilla, and R. Cywinski, Evidence for time-reversal symmetry breaking in the noncentrosymmetric superconductor $LaNiC_2$, Phys. Rev. Lett. **102**, 117007 (2009).
[23] E. M. Carnicom, W. Xie, T. Klimczuk, J. Lin, K. Gornicka, Z. Sobczak, N. P. Ong, and R. J. Cava, Sci. Adv. **4**, eaar7969 (2018).

[24] B. Joshi, A. Thamizhavel, and S. Ramakrishnan, Superconductivity in noncentrosymmetric BiPd, Phys. Rev. B **84**, 064518 (2011).

[25] M. N. Ali, Q. Gibson, T. Klimczuk, and R. J. Cava, A noncentrosymmetric superconductor with a bulk 3D Dirac cone gaped by strong spin orbit coupling, Phys. Rev. B **89**, 020505(R) (2014).

[26] T.-R. Chang, P.-J. Chen, G. Bian, S.-M. Huang, H. Zheng, T. Neupert, R. Sankar, S.-Y. Xu, I. Belopolski, G. Chang, Bao Kai Wang, F. Chou, A. Bansil, H.-T. Jeng, H. Lin, and M. Zahid Hasan, Topological Dirac surface states and superconducting pairing correlations in $PbTaSe_2$, Phys. Rev. B **93**, 245130 (2016).

[27] S. Y. Guan, P. J. Chen, M. W. Chu, R. Sankar, F. Chou, H. T. Jeng, C. S. Chang, and T. M. Chuang, Superconducting topological surface states in the noncentrosymmetric bulk superconductor $PbTaSe_2$, Sci. Adv. **2**, e1600894 (2016).

[28] T. Mizushima, A. Yamakage, M. Sato, and Y. Tanaka, Dirac-fermion-induced parity mixing in superconducting topological insulators, Phys. Rev. B **90**, 184516 (2014).

[29] U. Kaluarachchi, Y. Deng, M. F. Besser, K. Sun, L. Zhou, M. Cuong Nguyen, Z. Yuan, C. Zhang, J. S. Schilling, M. J. Kramer, S. Jia, C.-Z. Wang, K.-M. Ho, P. C. Canfield, and S. L. Budko, Highly responsive ground state of $PbTaSe_2$: Structural phase transition and evolution of superconductivity under pressure, Phys. Rev. B **95**, 224508 (2017).

[30] C. Q. Xu, R. Sankar, W. Zhou, Bin Li, Z. D. Han, B. Qian, J. H. Dai, Hengbo Cui, A. F. Bangura, F. C. Chou, and X. Xu, Topological phase transition under pressure in the topological nodal line superconductor $PbTaSe_2$, Phys. Rev. B **96**, 064528 (2017).

[31] R. Sankar, G. Narsinga Rao, I. Panneer Muthuselvam, G. Bian, H. Zheng, G. Peng-Jen Chen, T.-R. Chang, S. Xu, G. Senthil Murgan, C.-H. Lin, W.-L. Lee, H.-T. Jeng, M. Zahid Hasan, and F.-C. Chou, Single crystal growth and physical property characterization of $PbTaSe_2$ as a noncentrosymmetric type-II superconductor, arXiv:1511.05295.

[32] Y.-J. Long, L.-X. Zhao, P.-P. Wang, H.-X. Yang, J.-Q. Li, H. Zi, Z.-A. Ren, C. Ren, G.-F. Chen, Single crystal growth and physical property characterization of non-centrosymmetric Superconductor $PbTaSe_2$, Chin. Phys. Lett. **33**, 037401 (2016).

[33] P. Monthoux and G. G. Lonzarich, Magnetically mediated superconductivity in quasi-two and three dimensions, Phys. Rev. B **63**, 054529 (2001).

[34] Harada, J. J. Zhou, Y. G. Yao, Y. Inada, and Guo-qing Zheng, Abrupt enhancement of noncentrosymmetry and appearance of a spin-triplet superconducting state in $Li_2(Pd_{1-x}Pt_x)_3B$ beyond $x = 0.8$, Phys. Rev. B **86**, 220502(R) (2012).

[35] X. Lu, F. Ronning, P. H. Tobash, K. Gofryk, E. D. Bauer, and J. D. Thompson, Pressure-tuned point-contact spectroscopy of URu_2Si_2 from hidden order to antiferromagnetic states: Similarity of the Fermi surface gapping, Phys. Rev. B **85**, 020402(R) (2012).

[36] R. S. Gonnelli, D. Daghero, M. Tortello, G. A. Ummarino, Z. Bukowski, J. Karpinski, P. G. Reuvekamp, R. K. Kremer, G. Profeta, K. Suzuki, and K. Kurok, Fermi-surface topological phase transition and horizontal order parameter nodes in $CaFe_2As_2$ under pressure, Sci. Rep. **6**, 26394 (2016).

[37] H. Zi, L.-X. Zhao, X.-Y. Hou, L. Shan, Z. Ren, G.-F. Chen, and C. Ren, Pressure-dependent point-contact spectroscopy of superconducting $PbTaSe^2$ single crystals, Chin. Phys. Lett. **37**, 097403 (2020).

[38] R. S. Gonnelli, D. Daghero, G. A. Ummarino, V. A. Stepanov, J. Jun, S. M. Kazakov, and J. Karpinski, Direct evidence for two-band superconductivity in MgB_2 single crystals from directional point-contact spectroscopy in magnetic fields, Phys. Rev. Lett. **89**, 247004 (2002).

[39] See Supplemental Material at http://link.aps.org/supplemental/10.1103/PhysRevB.109.064510, which includes Refs. [37,40–43], for details on point-contact sample preparation, a set of point-contact Andreev reflection spectral data of junction J2, and estimation of the effective junction size, compared with the mean free path l_{fr} of $PbTaSe_2$ crystals.

[40] G. E. Blonder and M. Tinkham, Metallic to tunneling transition in Cu-Nb point contacts, Phys. Rev. B **27**, 112 (1983).

[41] G. Wexler, The size effect and the non-local Boltzmann transport equation in orifice and disk geometry, Proc. Phys. Soc. **89**, 927 (1966).

[42] Yu. G. Naidyuk, O. E. Kvitnitskaya, N. V. Gamayunova, D. L. Bashlakov, L. V. Tyutrina, G. Fuchs, R. Huhne, D. A. Chareev, and A. N. Vasiliev, Superconducting gaps in FeSe studied by soft point-contact Andreev reflection spectroscopy, Phys. Rev. B **96**, 094517 (2017).

[43] X. Lu, W. K. Park, S. Yeo, K.-H. Oh, S.-I. Lee, S. L. Bud'ko, P. C. Canfield, and L. H. Greene, Superconducting order parameter in nonmagnetic borocarbides RNi_2B_2C ($R = Y, Lu$) probed by point-contact Andreev reflection spectroscopy, Phys. Rev. B **83**, 104519 (2011).

[44] Y. Naidyuk, O. Kvitnitskaya, D. Bashlakov, S. Aswartham, I. Morozov, I. Chernyavskii, G. Fuchs, S.-L. Drechsler, R. Hühne, K. Nielsch, B. Büchner, and D. Efremov, Surface superconductivity in the Weyl semimetal $MoTe_2$ detected by point contact spectroscopy, 2D Mater. **5**, 045014 (2018).

[45] M. Mondal, B. Joshi, S. Kumar, A. Kamlapure, S. C. Ganguli, A. Thamizhave, S. S. Mandal, S. Ramakrishnan, and P. Raychaudhuri, Andreev bound state and multiple energy gaps in the noncentrosymmetric superconductor BiPd, Phys. Rev. B **86**, 094520 (2012).

[46] H. Wang, H.-C. Wang, H.-W. Liu, H. Lu, W.-H. Yang, S. Jia, X.-J. Liu, X.-C. Xie, J. Wei, and J. Wang, Observation of superconductivity induced by a point contact on 3D Dirac semimetal Cd_3As_2 Crystals, Nat. Mater. **15**, 38 (2016).

[47] S. Sasaki, M. Kriener, K. Segawa, K. Yada, Y. Tanaka, M. Sato, and Y. Ando, Phys. Rev. Lett. **107**, 217001 (2011).

[48] S.-Y. Xu, N. Alidoust, I. Beloplski, A. Richardella, C. Liu, M. Neupane, G. Bian, Song-Hsun, R. Sankar, C. Fang, B. Dellabetta, W. Dai, Q. Li, M. J. Gilbert, F. Chou, N. Samarth, and M. Zahid Hasan, Momentum-space imaging of Cooper pairing in a harlf Dirac-gas topological superconductors, Nat. Phys. **10**, 943 (2014).

[49] P. Zhang, K. Yaji, T. Hashimoto, Y. Ota, T. Kondo, K. Okazaki, Z. Wang, J. Wen, G. D. Gu, H. Ding, S. Shin, Observation of topological superconductivity on the surface of an iron-based superconductor, Science **360**, 182 (2018).

[50] W. Liu, L. Cao, S. Zhu, L. Kong, G. Wang, M. Papaj, P. Zhang, Y.-B. Liu, H. Chen, G. Li, F. Yang, T. Kondo, S. Du, G.-H. Cao, S. Shin, L. Fu, Z. Yin, H.-J. Gao, and H. Ding, A new Majorana

platform in an Fe-As bilayer superconductors, Nat. Commun. **11**, 5688 (2020).

[51] C.-K. Chiu, W. S. Cole, and S. Das Sarma, Induced spectral gap and pairing correlations from superconducting proximity effect, Phys. Rev. B **94**, 125304 (2016).

[52] G. E. Blonder, M. Tinkham, and T. M. Klapwijk, Transition from metallic to tunneling regimes in superconducting microconstrictions: Excess current, charge imbalance, and supercurrent conversion, Phys. Rev. B **25**, 4515 (1982).

[53] Y. Tanaka and S. Kashiwaya, Theory of tunneling spectroscopy of *d*-wave superconductors, Phys. Rev. Lett. **74**, 3451 (1995).

[54] J. Zhu, Z.-X. Yang, X.-Y. Hou, T. Guan, Q.-T. Zhang, Y.-Q. Li, X.-F. Han, J. Zhang, C.-H. Li, L. Shan, G.-F. Chen, and C. Ren, Tunneling spectroscopy of Al/AlO_x/Pb subjected to hydrostatic pressure, Appl. Phys. Lett. **106**, 202601 (2015).

[55] A. P. Schnyder, P. M. R. Brydon, D. Manske, and C. Timm, Andreev spectroscopy and surface density of states for a three-dimensional time-reversal-invariant topological superconductor, Phys. Rev. B **82**, 184508 (2010).

[56] N. Wennerdal and M. Eschrig, Theory of surface spectroscopy for noncentrosymmetric superconductors, Phys. Rev. B **95**, 024513 (2017).

[57] S.-I. Suzuki, Y. Kawaguchi, and Y. Tanaka, Local density of states in two-dimensional topological superconductors under a magnetic field: Signature of an exterior Majorana bound state, Phys. Rev. B **97**, 144516 (2018).